

# Instantaneous polarization attributes in the time–frequency domain and wavefield separation

M.S. Diallo,<sup>1\*</sup> M. Kulesh,<sup>1</sup> M. Holschneider<sup>1</sup> and F. Scherbaum<sup>2</sup>

<sup>1</sup>Institute for Mathematics, University of Potsdam, Am neuen Palais 10, 14469 Potsdam, and <sup>2</sup>Institute for Geoscience, University of Potsdam, Karl-Liebknecht Strasse 24–25, 14414 Potsdam, Germany

Received October 2004, revision accepted March 2005

## ABSTRACT

We introduce a method of wavefield separation from multicomponent data sets based on the use of the continuous wavelet transform. Our method is a further generalization of the approach proposed by Morozov and Smithson, in that by using the continuous wavelet transform, we can achieve a better separation of wave types by designing the filter in the time–frequency domain. Furthermore, using the instantaneous polarization attributes defined in the wavelet domain, we show how to construct filters tailored to separate different wave types (elliptically or linearly polarized), followed by an inverse wavelet transform to obtain the desired wave type in the time domain. Using synthetic and experimental data, we show how the present method can be used for wavefield separation.

## INTRODUCTION

Multicomponent seismic records contain important information about the subsurface that is very often overlooked because of the lack of appropriate tools for its extraction and interpretation. Vidale (1986), Rene *et al.* (1986) and Li and Crampin (1991) defined instantaneous polarization attributes for the characterization of Rayleigh waves and the observation of shear-wave splitting. Both methods were applied to two-component data and cannot be easily extended to higher-component data (Morozov and Smithson 1996). However, Morozov and Smithson (1996) proposed a method based on variational principles that allows generalization to any number of components, and they briefly addressed the possibility of using the instantaneous polarization attributes for wavefield separation and shear-wave splitting identification. Park (1987) proposed techniques that provide the polarization estimates in the frequency domain. The common characteristics of the methods mentioned above is that they all operate exclusively either in the time domain or in the frequency domain. However, when several wave-type arrivals are observed

at around the same time in a record, it becomes difficult to characterize the polarization attributes of the separate arrivals using methods that operate exclusively either in the time domain or in the frequency domain.

To solve this problem, the development of techniques that simultaneously handle the time and frequency dependence of the polarization attributes is needed. Reading, Mao and Gubbins (2001) designed a polarization filter following the method of Samson and Olson (1981). The method consists of applying a Fourier transform to successive segments of the three-component input data. The frequency-dependent eigenvalues (eigenvectors) are then computed from a  $3 \times 3$  spectral matrix in each segment and used for the construction of a polarization filter designed only in the frequency domain.

A better way of including the time–frequency relationship in polarization analysis would be to use the continuous wavelet transform. Such an approach, recently proposed by Diallo *et al.* (submitted to *Geophysics*), overcomes some of the difficulties mentioned above but is limited to two-component records. Here, we extend the method of Morozov and Smithson (1996) to the time–frequency domain, in order to use the instantaneous attributes for filtering, wavefield separation and shear-wave splitting investigation for any number of components.

---

\*E-mail: mamadou@math.uni-potsdam.de

## INSTANTANEOUS POLARIZATION ATTRIBUTES

### Time domain

Let  $\mathbf{S}(t) = (S_x(t), S_y(t), S_z(t))^T$  be a seismic vector describing the three-component seismic signal recorded from three orthogonal directions  $x$ ,  $y$  and  $z$ . Let  $\mathbf{S}^c = (S_x^c(t), S_y^c(t), S_z^c(t))^T$  be the analytic multicomponent signal obtained by using the Hilbert transform, in which the negative frequency part of the signal is zero and the positive frequency part is doubled:

$$\mathbf{S}^c(t) = \mathbf{S}(t) + i\mathbf{S}^H(t),$$

where  $(\cdot)^H$  indicates the Hilbert transform. The elements of the analytic multicomponent signal are given explicitly as

$$S_k^c(t) = S_k(t) + iS_k^H(t), \quad k = x, y, z.$$

Morozov and Smithson (1996) showed that the determination of the polarization attributes of  $\mathbf{S}(t)$  can be achieved by finding the phase factor  $\phi(t)$  in the expression,

$$\mathbf{S}^c(t) = \mathbf{A}(t)e^{i\phi(t)},$$

where  $\phi(t)$  is the unique real-valued phase of the multicomponent signal responsible for the fast time variation and  $\mathbf{A}(t)$  is the slow time-varying complex-valued vector function that contains the polarization, the amplitude and time phase-shift information of the multicomponent signal. The phase function is determined through a variational approach that maximizes the following functional:

$$\Phi(e^{-i\phi}\mathbf{S}^c(t)) = \sum_k \Re(e^{-i\phi}S_k^c(t))^2 + \varepsilon \left( \sum_k \Re(e^{-i\phi}S_k^c(t)) \right)^2,$$

where  $\Re(\cdot)$  indicates the real part of the argument and  $\varepsilon \ll 1$  is a regularization parameter to stabilize the calculation when the first term becomes constant.

The phase function  $\phi(t) = \phi_0(t)$  that maximizes the above functional is given by (Morozov and Smithson 1996)

$$\phi_0(t) = \frac{1}{2} \arg [B(t) + \varepsilon C(t)] + \pi n, \quad n \in \mathbb{N},$$

where

$$B(t) = \frac{1}{2} \sum_k S_k^c(t)^2, \quad C(t) = \frac{1}{2} \left( \sum_k S_k^c(t) \right)^2.$$

Given the phase factor  $\phi_0(t)$ , the instantaneous vectors for the semi-major axis  $\mathbf{R}(t)$  and the semi-minor axis  $\mathbf{r}(t)$  of an ellipse lying in a plane in 3D space, and the amplitude of the

multicomponent signal  $\mathbf{A}(t)$ , are derived as

$$\mathbf{R}(t) = \Re [e^{-i\phi_0(t)}\mathbf{S}^c(t)],$$

$$\mathbf{r}(t) = \Re [e^{-i(\phi_0(t)+\pi/2)}\mathbf{S}^c(t)],$$

$$\mathbf{A}(t) = \sqrt{\Phi(e^{-i\phi_0(t)}\mathbf{S}^c(t))}.$$

Other parameters, such as the ellipticity ratio, the dip angle, the strike angle and the phase difference, can then be easily calculated from the semi-minor and semi-major axes,  $\mathbf{r}(t)$  and  $\mathbf{R}(t)$ , respectively. Note that, since the phase  $\phi_0(t)$  is determined with an uncertainty modulo  $n\pi$ , the orientation of the axes is unknown.

### Time–frequency domain

The wavelet transform of a signal  $S(t) \in L^2(\mathbb{R})$  with respect to a mother wavelet  $g(t)$  is defined as

$$\mathcal{W}_g S(b, a) = \int_{-\infty}^{+\infty} \frac{1}{a} g^* \left( \frac{t-b}{a} \right) S(t) dt = \langle g_{b,a}, S \rangle, \quad (1)$$

where  $\langle \cdot, \cdot \rangle$  is the  $L^2$ -scalar product and  $g_{b,a}(t) = \frac{1}{a} g((t-b)/a)$  is generated from  $g$  through dilation ( $a > 0$ ) and translation ( $b \in \mathbb{R}$ ). The symbol  $(\cdot)^*$  denotes the complex conjugate. Applying (1) to  $\mathbf{S}(t)$  component-wise, yields  $\mathcal{W}_g \mathbf{S}(b, a)$  which consists of the respective wavelet transforms  $\mathcal{W}_g S_k(b, a)$  of  $S_k(t)$ . The wavelet  $g$  is assumed to be a function localized in the time and frequency domains, obeying the oscillation condition,

$$\int_{-\infty}^{+\infty} g(t) dt = 0.$$

The wavelet transform can be expressed in terms of the Fourier transform  $\hat{S}$  of  $S$  as

$$\mathcal{W}_g S(b, a) = \int_{-\infty}^{+\infty} \hat{g}^*(a\zeta) e^{2\pi i b\zeta} \hat{S}(\zeta) d\zeta.$$

From this result, we see that the inverse  $1/a$  of the scale may be associated with a frequency measured in units of the central frequency of  $g$ . If the central frequency of the wavelet is assumed to be  $f_0$ , then each scale  $a$  can be related to the physical frequency  $f$  by  $a = f_0/f$ . Therefore, if we select a wavelet with a unit central frequency, we can obtain the physical frequency directly by taking the inverse of the scale. For the sake of clarity, we consider a wavelet with unit central frequency and proceed with the physical frequency instead of the scale in the next sections. The multicomponent signal  $\mathbf{S}(t)$  can be recovered from its wavelet transform (again component-wise) as follows:

$$\mathbf{S}(t) = \frac{1}{C_g} \int_0^\infty \int_{-\infty}^{+\infty} \frac{1}{a} g \left( \frac{t-b}{a} \right) \mathcal{W}_g \mathbf{S}(b, a) \frac{db da}{a},$$

where the constant  $C_g$  is defined below.

Here, we consider only real-valued signals and admissible progressive analysing wavelets, i.e. we assume  $\hat{g}(f) = 0$  for  $f \leq 0$  and that the constant  $C_g = \int_0^\infty |\hat{g}(f)|^2 \frac{df}{f}$  is finite. With this restriction, the wavelet transform of the multicomponent signal  $\mathbf{S}(t)$  is equivalent to the wavelet transform of the multicomponent analytical signal  $\mathbf{S}^c(t)$  (Holschneider 1995).

Following the approach outlined in the previous section, it is possible to redefine all the instantaneous attributes in the time–frequency domain in terms of  $\mathcal{W}_g \mathbf{S}(b, a)$  and  $\phi_0(b, a)$ . The resulting semi-major axis, semi-minor axis and the instantaneous amplitude are

$$\begin{aligned} \mathbf{R}(b, a) &= \Re \left[ e^{-i\phi_0(b, a)} \mathcal{W}_g \mathbf{S}(b, a) \right], \\ \mathbf{r}(b, a) &= \Re \left[ e^{-i(\phi_0(b, a) + \pi/2)} \mathcal{W}_g \mathbf{S}(b, a) \right], \\ \mathbf{A}(b, a) &= \sqrt{\Phi(e^{-i\phi_0(b, a)} \mathcal{W}_g \mathbf{S}(b, a))}, \end{aligned} \quad (2)$$

respectively. The ellipticity ratio  $\rho(b, a)$  is then derived as

$$\rho(b, a) = \frac{\|\mathbf{r}(b, a)\|}{\|\mathbf{R}(b, a)\|}.$$

From (2), we have

$$\Re \mathcal{W}_g \mathbf{S}(b, a) = \mathbf{R}(b, a) \cos(\phi_0(b, a)) - \mathbf{r}(b, a) \sin(\phi_0(b, a)), \quad (3)$$

$$\Im \mathcal{W}_g \mathbf{S}(b, a) = \mathbf{R}(b, a) \sin(\phi_0(b, a)) + \mathbf{r}(b, a) \cos(\phi_0(b, a)). \quad (4)$$

Using (3) and (4), we can express the full wavelet transform  $\mathcal{W}_g \mathbf{S}(b, a)$  of the multicomponent signal in terms of the ellipticity parameters  $\mathbf{R}(b, a)$ ,  $\mathbf{r}(b, a)$  and the phase factors  $\phi_0(b, a)$  as

$$\mathcal{W}_g \mathbf{S}(b, a) = \Re \mathcal{W}_g \mathbf{S}(b, a) + i \Im \mathcal{W}_g \mathbf{S}(b, a). \quad (5)$$

The ellipse in 3D space is determined by the major axis which is well defined, except for a circular particle motion, in which case the presence of noise will introduce an artificial major axis. To avoid this problem, Schimmel and Gallart (2003) used the planarity vector,

$$\mathbf{p}(b, a) = \mathbf{R}(b, a) \times \mathbf{r}(b, a) = (p_x(b, a), p_y(b, a), p_z(b, a)),$$

for circular or elliptical motion, which should remain in the same direction if the ellipse remains in the same plane. To track the position of the ellipse in 3D space, we determine the different angles between  $\mathbf{p}$  and the orthogonal axes,  $x$ ,  $y$  and  $z$ , at each point  $(b, a)$ . We denote these angles,  $\theta_x(b, a)$ ,  $\theta_y(b, a)$  and  $\theta_z(b, a)$ , respectively, where

$$\theta_k(b, a) = \arccos \left( \frac{|p_k(b, a)|}{\|\mathbf{p}(b, a)\|} \right), \quad \theta_k(b, a) \in \left[ 0, \frac{\pi}{2} \right], \quad k = x, y, z. \quad (6)$$

Using  $\mathbf{R}(b, a)$ ,  $\mathbf{r}(b, a)$ ,  $\mathbf{p}(b, a)$  and other derived instantaneous polarization parameters, it is possible to design filters that enable wave types with specific polarization attributes to be selected or analysed. Applications may include surface-wave filtering/analysis, the investigation of shear-wave splitting, separation of converted waves, removal of out-plane energy, etc. To construct an efficient filter, previous techniques, mostly designed either in the time domain (Kanasewich 1981; Perelberg and Hornbostel 1994; Morozov and Smithson 1996; Shieh 1997) or in the frequency domain (Park 1987), can be revisited in the light of the present contribution.

## APPLICATION TO FILTERING

### Synthetic example

In the following we show how to use the instantaneous attributes defined in the wavelet domain for the purpose of separating different wave types. We simulate a three-component record with seismic events consisting of the superposition of elliptically and linearly polarized events. The simulation is not based on an actual physical model but is rather considered as a simplified illustration of the filtering principle. The actual simulated three-component record is shown in Fig. 1. It consists of an elliptically polarized event in the  $(x - y)$  plane between 1 s and 5 s, a second elliptically polarized event in the  $(x - z)$  plane between 5 s and 9 s, a third elliptically polarized event in the  $(y - z)$  plane between 9 s and 15 s and, finally, a mixture of linearly and elliptically polarized events having different frequency content between 15 s and 20 s. To extract an elliptically polarized event in any plane, we design a filter constrained by the range of reciprocal ellipticity and the direction of  $\mathbf{p}(b, a)$  as given by (6).

To isolate the elliptically polarized event in the  $(x - y)$  plane, we first identify the region in the time–frequency plane where  $\theta_z(b, a) = 0$ . This is between 1 s and 5 s in time in Fig. 2(d), corresponding to the ellipticity ratio in the same time window in Fig. 2(a) and where the reciprocal ellipticity ratio  $\rho(b, a)$  is within a certain range (i.e.  $\rho(b, a) \approx 0.6$  in the present example as shown in Fig. 2a). Note that the linear event is not observed here because its ellipticity ratio is zero and corresponds to the background colour for this plot.

Next we set the values of  $\mathbf{R}(b, a)$ ,  $\mathbf{r}(b, a)$  and  $\phi_0(b, a)$  that fall outside the region delimited by the two previous concurrent

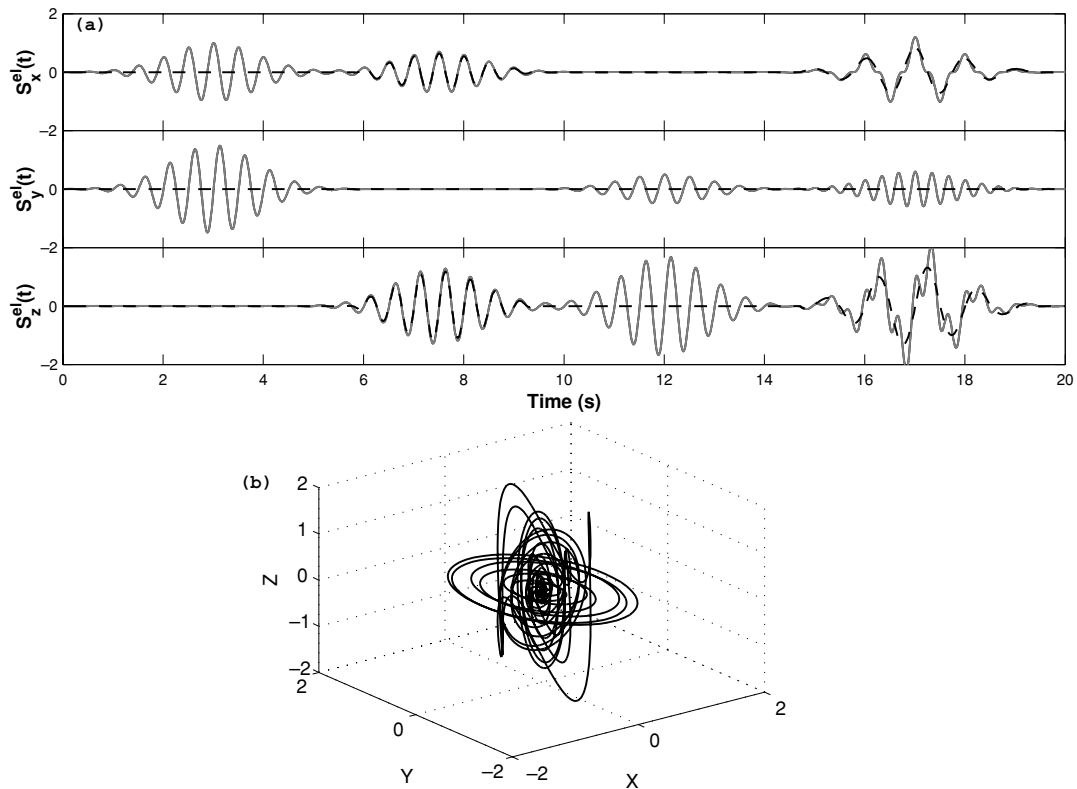


**Figure 1** (a) Three synthetic signals simulating a three-component record with elliptically polarized events contained in the  $(x - z)$ ,  $(x - y)$  and  $(y - z)$  planes. The late arrival on the three seismograms is a mixture of a linearly polarized event and an elliptically polarized event with different frequency content. (b) Hodogram plot showing the ellipses in the different polarization planes.

constraints to zero, and substitute the resulting parameters  $\mathbf{R}'(b, a)$ ,  $\mathbf{r}'(b, a)$  and  $\phi'_0(b, a)$  into (4) and (3). Finally, the inverse-wavelet transform of (5) yields the multicomponent signal that defines the desired event. The procedure outlined above can be adapted to extract the elliptically polarized events in the  $(x - y)$  and  $(y - z)$  planes. In Fig. 1(a), we have chosen to detect the events in the  $(x - z)$  plane, where from the initial synthetic seismogram we have one distinguishable elliptical event that extends from nearly 5 s to 10 s, and also the elliptical event in the time window between 15 s and 20 s which is superimposed the linear event. The dashed curves in Fig. 1(a) depict the filtering results which replicate the initial synthetic fairly well, as desired.

### Experimental data

The real seismograms (Fig. 3) used in this study are a three-component record from an explosive-source experiment aimed at imaging the Dead Sea Transform in the Middle East (DESERT Group 2000). The horizontal seismograms were rotated into radial and transverse components using the

shot/receiver azimuth obtained from the survey geometry. The methodology described in the previous section was applied to these seismograms to produce the polarization attributes in the time–frequency domain. The modulus of the wavelet transforms of each individual component of the record is shown in Fig. 4, which depicts the location of some strong events (surface waves) in the time–frequency plane and the relative importance of their energy content, indicated by the grey scale (from white for low-amplitude to black for high-amplitude arrivals).

Figure 5 shows the polarization attributes used to illustrate the approach to filtering the real seismograms in Fig. 3. Figure 5(a) corresponds to the reciprocal ellipticity which is normally close to one for either elliptically or circularly polarized events and to zero for linearly polarized events. A window of persistent elliptical polarization can be observed between approximately 3 s and 5 s in time, culminating around 5 Hz on the frequency axis. With the help of the direction of the planarity vector, indicated by the different angles  $\theta_k(b, a)$ ,  $k = x, y, z$  in Figs 5(b,c,d), respectively, we can determine the direction of the energy arrival at each point  $(b, a)$ .

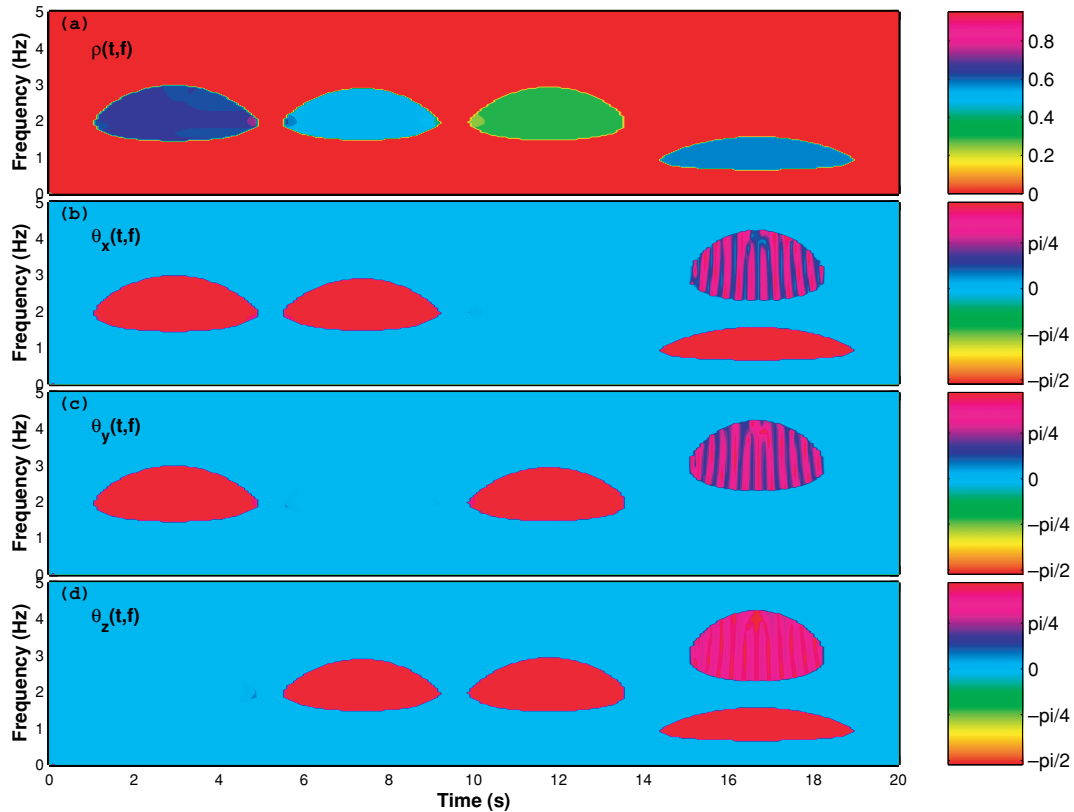


**Figure 2** Instantaneous polarization attributes in the time–frequency domain: (a) the ellipticity ratio for the different events in the multicomponent signal; (b) the angle between the planarity vector and the  $x$ -axis; (c) the angle between the planarity vector and the  $y$ -axis; (d) the angle between the planarity vector and the  $z$ -axis. Note that for the first event,  $\theta_z(b, a) = 0$ ; for the second event,  $\theta_y(b, a) = 0$ ; for the third event,  $\theta_x(b, a) = 0$ . Only the linearly polarized event (high frequency) between 14 s and 20 s has non-zero components for  $\mathbf{p}$  in all directions. For the elliptically polarized event in that time window  $\theta_y(b, a) = 0$ .

Figure 5(b) shows two regions in the earlier arrival times (marked with labelled arrows), where  $\theta_x(b, a)$  is relatively small. The first region is contained in a narrow frequency strip that extends from 2 s to nearly 4 s and would correspond to the lower frequency region with events of low elliptical polarization as can be seen in the corresponding time–frequency window (Fig. 5a). The second region covers a wider frequency range from 4 Hz to 10 Hz and is limited to the time window between 2.5 s and 4 s. The arrivals in this region are linearly polarized as indicated by the small value of  $\rho(b, a)$  in that region (Fig. 5a). The weak  $\theta_x(b, a)$  values in this region suggests that the direction of incoming energy is predominantly in the  $(y - z)$  plane.

In Fig. 5(c), the region (marked with a labelled arrow) that would correspond to the energy event with elliptical polarization mentioned previously is predominantly blue to light blue, corresponding to small angles  $\theta_y(b, a)$ , which means that the planarity vector is nearly parallel to the  $y$ -axis in that region.

This behaviour can be interpreted as an indication that the energy arrival in the time–frequency window under observation is mostly contained in the  $(x - z)$  plane.

By performing this kind of analysis on multicomponent data, it is easy to identify the out-of-plane energy arrivals and construct appropriate filters to reduce the contamination of the radial and vertical components.

Figure 6(a) illustrates how the information from  $\rho(b, a)$  and  $\theta_k(b, a)$  can be used for wave-type filtering. This figure shows a seismic arrival with a polarization in the horizontal  $(x - y)$  plane. It was obtained by selecting the region in the time–frequency plane where  $\theta_z(b, a)$  is relatively small and then setting the corresponding parameters  $\mathbf{R}(b, a)$  and  $\mathbf{r}(b, a)$  to zero, followed by an inverse transform as was performed with the synthetic example. With the result from only one seismogram, it is difficult to speculate about the nature of the signal in such multicomponent seismograms. Because of the nature of the source used in the experiment (explosive), shear-wave

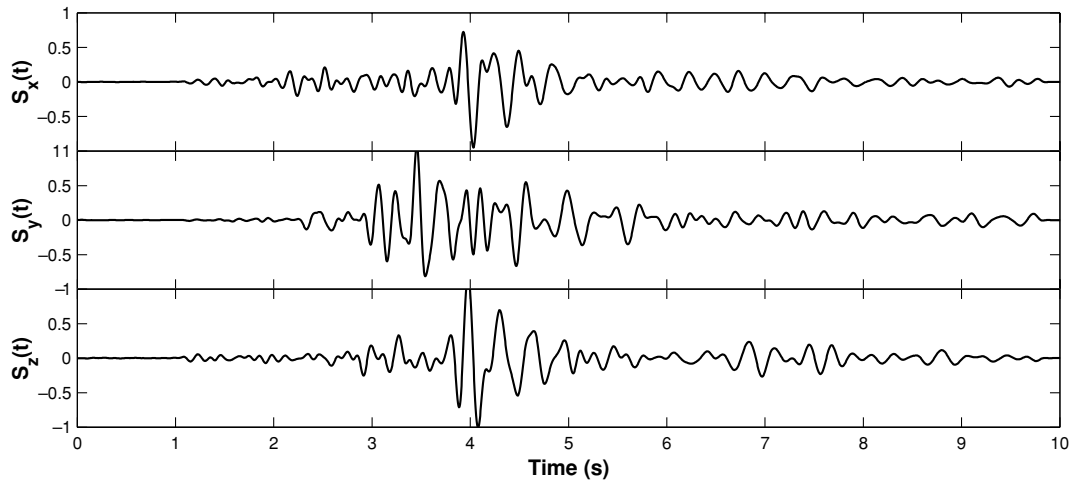


Figure 3 Three-component real seismograms showing radial, transverse and vertical components. The strong surface-wave arrivals can be observed between 3 s and 5 s.

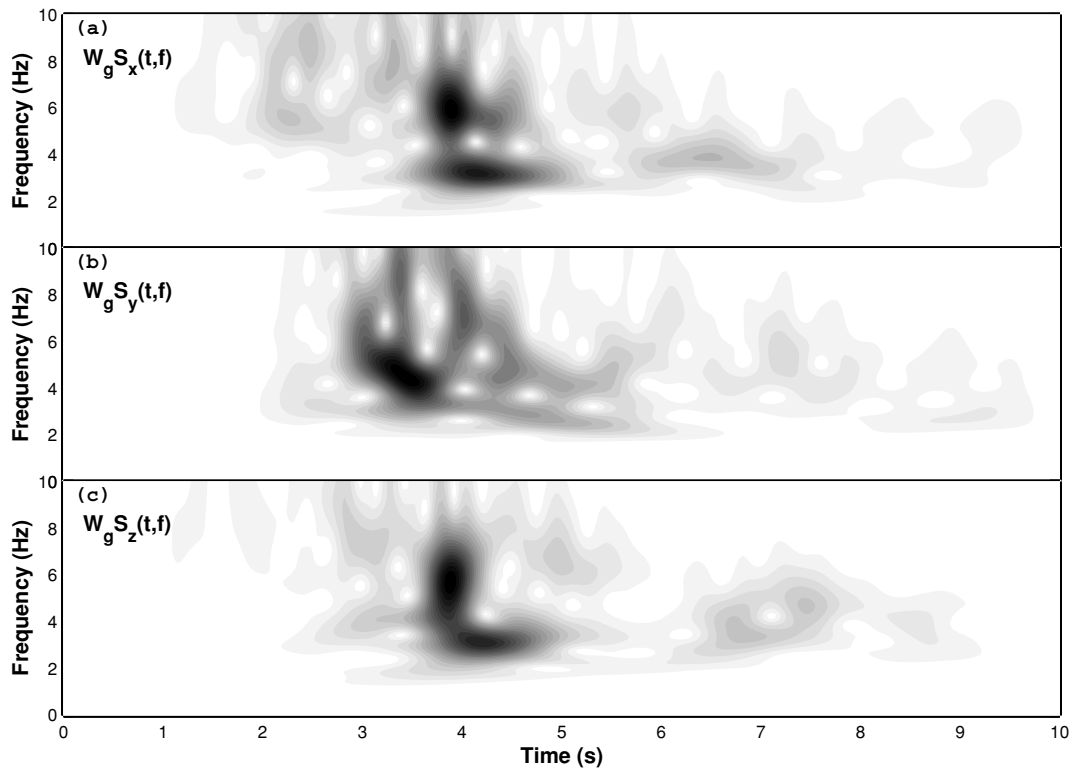
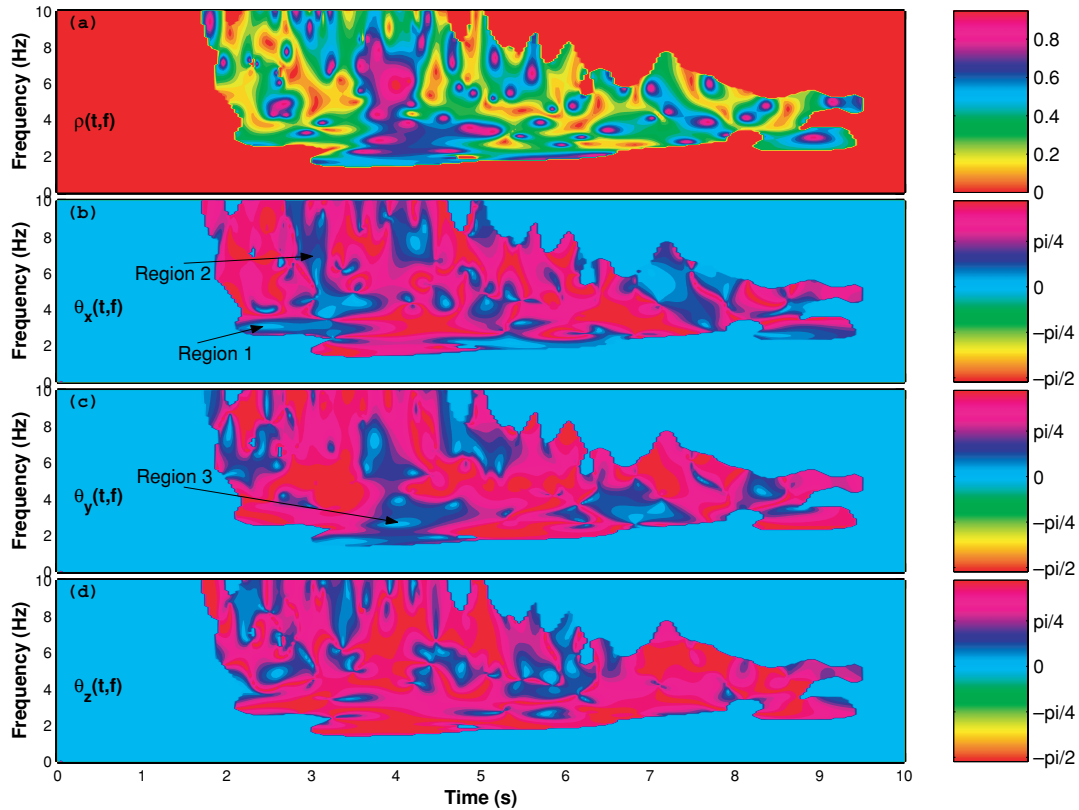


Figure 4 Wavelet transform moduli of the different signals in Fig. 3. Strong energy arrivals that can be associated with the Rayleigh-wave arrivals can be observed on (a) and (c) between approximately 3.8 s and 5 s.

arrivals would be relatively weak. The strong arrival observed on the filtered seismogram would probably correspond to P-to-S conversion or to P-wave energy leaking into the horizontal component due to the offset. It is important to note that the energy arrival from the filtered vertical component is very weak, which suggests that our filter is capable of detect-

ing the desired signal, expected to consist mainly of the  $x$ - and  $y$ -components.

Another important application of polarization analysis is the removal of out-of-plane energy, which is important in geologically complex areas. These out-of-plane energy arrivals may contaminate the radial component, which adds to the



**Figure 5** Instantaneous polarization parameters used for the wave-type separation: (a) the reciprocal ellipticity; (b) the angle between the direction of the planarity vector and the  $x$ -axis; (c) the angle between the direction of the planarity vector and the  $y$ -axis; (d) the angle between the direction of the planarity vector and the  $z$ -axis.

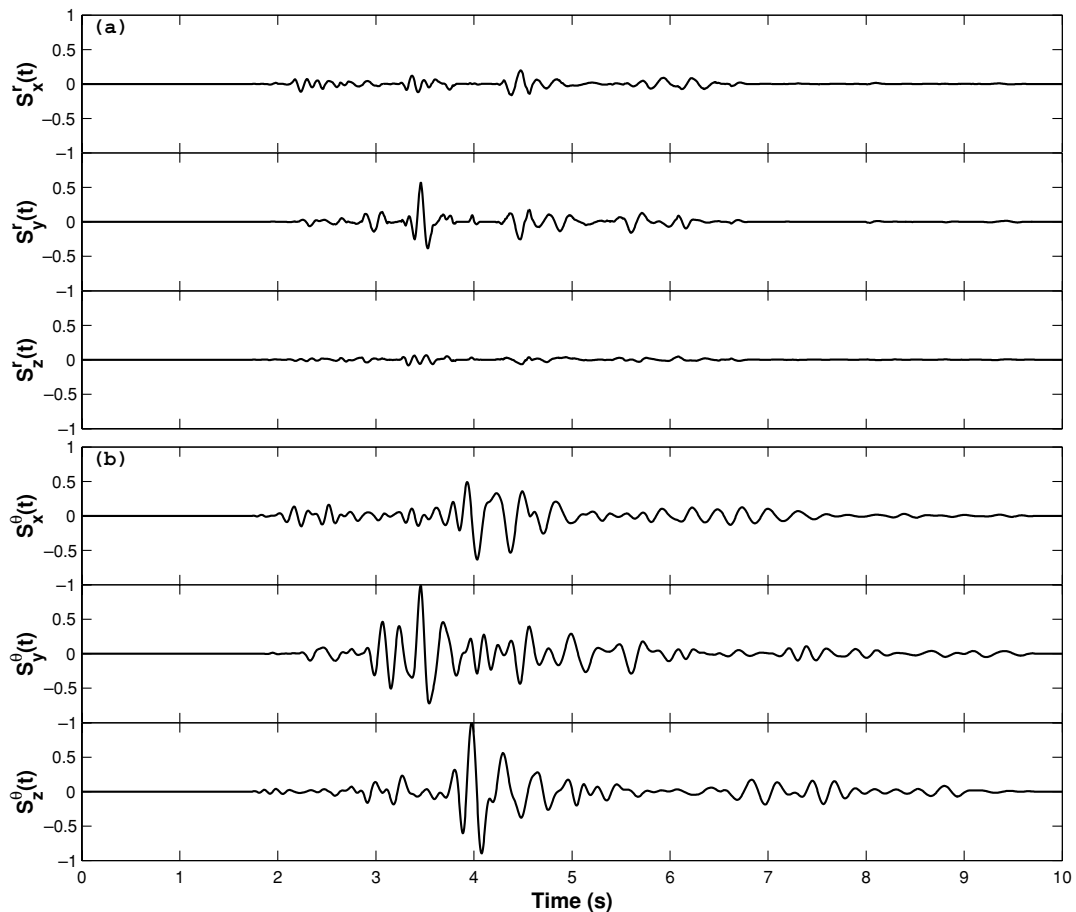
difficulty of its analysis and may lead to errors in the subsequent interpretation. By using the cosine directions  $\theta_k(b, a)$ , much of this energy can be attenuated. This is achieved by first normalizing the different  $\theta_k(b, a)$  so that the range of each  $\theta_k(b, a)$  is between 0 and 1. Each normalized  $\theta_k(b, a)$  is then multiplied by the wavelet transform of the signal component along the corresponding  $k$ -axis ( $k = x, y, z$ ), followed by an inverse wavelet transform.

Figure 6(b) illustrates the application of this approach to the multicomponent signal in Fig. 3, using the normalized  $\theta_x(b, a)$ ,  $\theta_x(b, a)$ ,  $\theta_z(b, a)$ , shown in Figs (5b–d), and the wavelet transforms of  $S_x(t)$ ,  $S_y(t)$ ,  $S_z(t)$ . It can be seen that the interference of the wavefield in the time window from nearly 2.5 s to 5 s has been reduced, making it much easier to identify the events in  $S_x(t)$  and  $S_z(t)$  that contribute to the Rayleigh-wave arrival (large amplitude, low frequency events around 4 s from both components). Also, the event that might correspond to the Love wave is clearly singled out in  $S_y(t)$  around 3.5 s in time. We note that the most important effect of the filter for this particular example, in terms of ampli-

tude reductions, is observed along  $S_y(t)$  at around 4 s. This would mean that around this time, an arrival with a relatively large amount of out-of-plane energy has been recorded along this component. This observation is consistent with the interpretation of  $\theta_y(b, a)$ , which has low values around this time window, indicating that the arrivals are mostly from the  $x$ - and  $z$ -directions.

## CONCLUSIONS

We have used the continuous wavelet transform to extend the polarization analysis technique for multicomponent data, initially proposed by Morozov and Smithson (1996), into the time–frequency domain. We have discussed prospective methods for wave-type separation, based on the use of the reciprocal ellipticity and the planarity vector. The introduction of the time–frequency domain into the polarization analysis method can improve the performance of existing techniques used for wave-type separation, surface-wave analysis, directional filtering and investigation of shear-wave splitting.



**Figure 6** Example of wave-type separation applied to the three-component seismograms in Fig. 3. (a) Application of the polarization filter to identify the seismic events with pure polarization in  $(x - y)$ . Note the low amplitudes on the filtered vertical component. (b) Filtered three-component seismograms resulting from the multiplication of the wavelet transforms of each component by the corresponding normalized cosine direction of the planarity vector followed by an inverse wavelet transform. This filtering has the effect of reducing the influence of energy arrivals that come from directions not parallel to the direction in which each component is most sensitive to particle motion.

## ACKNOWLEDGEMENTS

This project was supported by a grant from the Deutsche Forschungsgemeinschaft (DFG) within the framework of the priority program SPP 1114: ‘Mathematical methods for time series analysis and digital image processing’. In the subsection ‘Experimental data’, we used data from the Controlled Source Array (CSA) experiment as part of the Dead Sea Research Project (DESERT, <http://www.gfz-potsdam.de/pb2/pb22/projects/deadsea/ds-home.html>). DESERT was financed by the Deutsche Forschungsgemeinschaft (DFG), the Geoforschungszentrum Potsdam (GFZ) and the Minerva Foundation. Instruments were provided by the Geophysical Instru-

ment Pool Potsdam (GFZ) and the Free University of Berlin. We thank the anonymous reviewers for their valuable comments and suggestions that were very helpful in improving the content of the manuscript.

## REFERENCES

- DESERT Group 2000. Multinational geoscientific research kicks off in the Middle East. *EOS*, **81**(50), 609, 616–617.
- Holschneider M. 1995. *Wavelets: an Analysis Tool*. Clarendon Press, Oxford.
- Kanasewich E.R. 1981. *Time Series Sequence Analysis in Geophysics*. University of Alberta Press, Edmonton, Alberta.

- Li X.L. and Crampin S. 1991. Complex component analysis of shear wave splitting: theory. *Geophysical Journal International*, **107**, 597–604.
- Morozov I.B. and Smithson S.B. 1996. Instantaneous polarization attributes and directional filtering. *Geophysics*, **61**, 872–881.
- Park J. 1987. Frequency dependent polarization analysis of high-frequency seismograms. *Journal of Geophysical Research*, **92**, 12664–12674.
- Perelberg A.I. and Hornbostel S.C. 1994. Application of seismic polarization analysis. *Geophysics*, **59**, 119–130.
- Reading A.M., Mao W. and Gubbins D. 2001. Polarization filtering for automatic picking of seismic data and improved converted phase detection. *Geophysical Journal International*, **147**, 227–234.
- Rene R.M., Fitter J.L., Forsyth P.M., Kim K.Y., Murray D.J., Walters J.K. and Westerman J.D. 1986. Multicomponent seismic studies using complex trace analysis. *Geophysics*, **51**, 1235–1251.
- Samson J.C. and Olson J.V. 1981. Data-adaptive polarization filter for multichannel geophysical data. *Geophysics*, **46**, 1423–1431.
- Schimmel M. and Gallart J. 2003. The use of instantaneous polarization attributes for seismic signal detection and image enhancement. *Geophysical Journal International*, **155**, 653–668.
- Shieh C.F. 1997. Estimation of shear-wave splitting using orthogonal transformation. *Geophysics*, **59**, 657–661.
- Vidale J.E. 1986. Complex polarization analysis of particle motion. *Bulletin of the Seismological Society of America*, **76**, 1393–1405.